



Effect of different sizes of bioactive glass-coated mesoporous silica nanoparticles on dentinal tubule occlusion and mineralization

Jae-Hyun Jung¹ · Soo-Byung Park¹ · Kyung-Hyeon Yoo² · Seog-Young Yoon² · Moon-Kyoung Bae³ · Dong Joon Lee⁴ · Ching-Chang Ko⁴ · Yong Hoon Kwon⁵ · Yong-Il Kim^{1,6} 

Received: 1 May 2018 / Accepted: 20 September 2018 / Published online: 30 September 2018
© Springer-Verlag GmbH Germany, part of Springer Nature 2018

Abstract

Objectives To synthesize two different sizes of bioactive glass-coated mesoporous silica nanoparticles (BGN@MSNs) and to investigate their effects on dentinal tubule occlusion and remineralization.

Materials and methods Two different sizes of mesoporous silica nanoparticles (MSNs) were synthesized using the Stöber method (368A, 1840A) and coated with bioactive glass nanoparticles (BGNs) using a modified quick alkali-mediated sol-gel method (368B, 1840B). Sensitive tooth disc models were prepared and divided into six groups and the following treatments were applied: group 1—no treatment, group 2—bioglass, group 3—368A, group 4—368B, group 5—1840A, and group 6—1840B. Then, five discs were selected from each group and soaked in 6 wt% citric acid to test acid resistance. Dentinal tubule occlusion and occlusion ratio were observed using field-emission scanning electron microscopy. In vitro mineralization tests using simulated body fluid solution were performed to evaluate the remineralization effect of the treatment.

Results All samples effectively occluded the dentinal tubule and formed a membrane-like layer. After acid treatment, 1840B (group 6) exhibited the highest rate of dentinal tubule occlusion. Remineralization was observed in 368B and 1840B, and 1840B exhibited the fastest remineralization.

Conclusions Dentinal tubule remineralization induced by the BGN@MSN biocomposite can be used to stabilize long-term prognosis in dentin hypersensitivity. The 1840B induced the most efficient remineralization, and its smaller size and larger surface area were effective for remineralization.

Clinical relevance The BGN@MSN biocomposite with its smaller size and larger surface area was more effective for remineralization and dentinal tubule sealing.

Keywords Bioactive glass · Mesoporous silica · Size · Surface area · Nanoparticle · Remineralization · Dentin hypersensitivity

Introduction

Dentin hypersensitivity (DH) is a common problem in dentistry, with a prevalence of 4–74% [1]. The most widely accepted

DH mechanism is the hydrodynamic theory proposed by Brännström [2]. Recently developed DH treatments have focused on the management of the hydrodynamic pain mechanism. Pain can be reduced either by reducing fluid flow in the

Yong Hoon Kwon and Yong-Il Kim contributed equally to this work.

✉ Yong Hoon Kwon
y0k0916@pusan.ac.kr

✉ Yong-Il Kim
kimyongil@pusan.ac.kr

¹ Department of Orthodontics, Dental Research Institute, Pusan National University Dental Hospital, Geumoro 20, Mulgeum, Yangsan 50612, South Korea

² School of Materials Science and Engineering, Pusan National University, Busandaehak-ro 63beon-gil, Geumjeong-gu, Busan 46241, South Korea

³ Department of Oral Physiology, School of Dentistry, Pusan National University, Busandaehak-ro 49, Mulgeum, Yangsan 50612, South Korea

⁴ Department of Orthodontics, School of Dentistry, University of North Carolina, Chapel Hill, NC 27599, USA

⁵ Department of Dental Materials, Pusan National University, Busandaehak-ro 49, Mulgeum, Yangsan 50612, South Korea

⁶ Institute of Translational Dental Sciences, School of Dentistry, Pusan National University, Busandaehak-ro 49, Mulgeum, Yangsan 50612, South Korea

dentinal tubules or by blocking nerve reactions in the pulp. Attempts have been made to reduce fluid flow in the dentinal tubules by physically or chemically altering the smear layer, closing the tubules, or by using desensitizing agents [3–6]. However, even if the tubules are closed, they can be re-exposed due to exposure to dietary acids, thereby shortening the effects of the desensitizing agents.

Bioactive glasses (BGs) emit sodium, calcium, and phosphate ions to raise the pH and create an ideal environment for remineralization [7]. BGs are effective for treating hypersensitivity by closing approximately 90% of the dentine tubules, but these closures have low strength and the smear layer is easily removed by brushing the tooth [8]. Mesoporous silica nanoparticles (MSNs), which are porous particles 50–300 nm in diameter with a spiracle of 2–6 nm, are also widely used as an ideal medium for drug, gene, and functional nanoparticles in the biomedical field due to its stable structure, large surface area, adsorption, and thermal and chemical stability [9, 10]. Tian et al. investigated the dentinal tubule closure and remineralization capability of Ca^{2+} - or $\text{PO}_4^{(3-)}$ -coated MSNs [11]. Our previous study also developed bioactive glass nanoparticle-coated mesoporous silica nanoparticles (BGN@MSNs) to reduce the reopening after acid challenges and improve dentinal tubule sealing, considering the large surface area of MSN and high bioactivity of BGN [12]. In the previous study of BG, the variation of mesoporous structure and the nanoparticle size increase the bonding properties [13, 14]. Therefore, it is expected that the smaller the particle size and the surface area grows, the dentin tubule occlusion and remineralization will increase. But insufficient studies have been performed regarding these subjects.

Thus, the purpose of this study was to synthesize BGN@MSNs of different sizes by coating BGN on mesoporous silica nanoparticles synthesized with various particle sizes to investigate the effect of particle size and surface area and to examine the effects of the different-sized BGN@MSNs on the occlusion and remineralization of dentinal tubules. The null hypothesis was that there were no differences of dentinal tubule occlusions and remineralizations according to the particle sizes of BGN@MSN.

Materials and methods

Synthesis of two different-sized BGN-coated MSNs

Two different-sized MSNs were synthesized according to the “Stöber method” described by Stöber et al. [15]. Briefly, 211 mg of cetyltrimethylammonium (CTAC, Sigma-Aldrich, St. Louis, MO, USA), 17.7 g of deionized water (DIW), 175 mL of methanol (99.9%), and 7.2 g of aqueous ammonia solution (28%) were mixed for 15 s at room temperature. Then, either 368 or 1840 μL of tetraethyl orthosilicate (TEOS, Sigma-Aldrich, St. Louis, MO, USA) was added to the solution and mixed for 3 s. The mixture was sealed and aged for 20 h at room temperature. After aging, it was washed with methanol (99.9%) and dried at 60 °C. Subsequently, the surfactant was removed by 10 h of calcination at 550 °C to obtain the MSN (diameter of 368A 300–400 nm, 1840A 150–250 nm).

The “quick alkali-mediated sol-gel method” of Xia et al. [16] was modified to coat the synthesized MSNs (368A, 1840A) with BGN. Briefly, 2.8 mL of 2 M HNO_3 , 13.9 mL of DIW, and 1.0 g of MSNs were added to 50 mL of ethanol and sonicated. Then, 21.6 mL of TEOS was added and vigorously stirred at room temperature for 30 min, and 2.2 mL of triethyl phosphate (TEP, Sigma-Aldrich, St. Louis, MO) was subsequently added and stirred for 30 min. Afterwards, 14.04 g of $\text{Ca}(\text{NO}_3)_2 \cdot 4\text{H}_2\text{O}$ was added and stirred for 30 min and 2 M NH_4OH was added until the pH reached 4.5. After aging at 60 °C for 24 h, the white precipitate was removed and ethanol was added, stirred, and dried in an oven at 80 °C. The final sample was obtained by calcination at 600 °C for 5 h (368B and 1840B). Table 1 summarizes the four samples.

Characterization of the different-sized BGN@MSNs

The synthesized MSNs and BGN@MSNs were characterized by X-ray diffraction (XRD) to determine the crystal state of the samples using an Ultima IV multipurpose XRD system (Rigaku, The Woodland, TX, USA) at 40 kV and 40 mA, with a scanning speed of 0.1°/min. Wide-angle XRD was

Table 1 Description of the samples

Samples	Synthesis method	Amount of TEOS (μL) in the Stöber method	Composition
368A	The Stöber method	368	MSN
368B	The Stöber and quick alkali-mediated sol-gel method	368	BGN-coated MSN
1840A	The Stöber method	1840	MSN
1840B	The Stöber and quick alkali-mediated sol-gel method	1840	BGN-coated MSN

performed in the 2θ range from 10 to 80° , and small-angle XRD was performed from 0.5 to 10° . The functional groups were examined using the attenuated total reflectance (ATR) method of the Fourier-transform infrared spectroscopy (FT-IR) on a spectrum GX FT-IR spectrometer (PerkinElmer Inc., Waltham, USA).

The N_2 adsorption-desorption isotherms were measured using an adsorption analyzer (autosorb-iQ; Quantachome, Boynton, FL, USA). The specific surface area and pore size distribution were measured by the Brunauer-Emmett-Teller (BET) and Barrett-Joyner-Halenda (BJH) methods, respectively. The morphology of the samples was observed using a 200-kV field-emission transmission electron microscope (200 kV FETEM, TALOS F200X; FEI, Hillsboro, OR, USA).

Size effects on in vitro dentin tubule occlusion and acid resistance stability

Fabrication of sensitive tooth samples

According to the protocol reviewed and approved by the Institutional Review Board of Pusan National University Dental Hospital (PNUDH-2016-033), 60 premolar teeth were collected after obtaining informed consent of the donors. The teeth were stored at 4°C in a 0.5% thymol solution and used within 1 month of collection. Dentin discs 1 mm in thickness were prepared perpendicular to the longitudinal axis of the tooth under the enamel-dentin junction with a low-speed diamond saw (Struers Accutom-50; Ballerup, Denmark). The discs were polished using 320- and 600-grit silicon carbide (SiC) polishing paper for 60 s each. Subsequently, the discs were soaked in 1 wt% citric acid solution for 20 s and washed completely with water to form a sensitive tooth model by opening the dentinal tubules of the disc [17].

Dentin tubule occlusion test

The samples were randomly divided into six groups as follows:

Group 1: No treatment (control)

Group 2: Slurry prepared at a ratio of 100 mg of Bioglass 45S5 (BG, 45 SiO_2 -24.5 CaO -24.5 Na_2O -6 P_2O_5 , 20–50 μm , Aladdin Industrial Corporation, Shanghai, China) was applied to the dentin surface at a low speed for 15 s using a rotary cup, then applied again for an additional 15 s so that the total application time was 30 s.

Group 3: Slurry prepared at a ratio of 100 mg 368A/200 μL deionized water was applied to the dentin surface in the same manner as described for Group 2.

Group 4: Slurry prepared at a ratio of 100 mg 368B/200 μL deionized water was applied to the dentin surface in the same manner as described for Group 2.

Group 5: Slurry prepared at a ratio of 100 mg 1840A/200 μL deionized water was applied to the dentin surface in the same manner as described for Group 2.

Group 6: Slurry prepared at a ratio of 100 mg 1840B/200 μL deionized water was applied to the dentin surface in the same manner as described for Group 2.

After each sample was prepared and rinsed thoroughly with deionized water, five randomly selected dentin discs ($n = 5$) were used for each group, and the remaining discs for were used for the acid resistance stability test ($n = 5$).

Acid resistance stability of occluded dentine tubules

After desensitizing treatment, five discs per group were soaked in 6 wt% citric acid solution (pH 1.5) for 60 s and were washed thoroughly with deionized water to confirm resistance to a strongly acid environment.

FESEM assessment of dentinal tubule occlusion and acid resistance stability

After storing the samples in a 100% humidified atmosphere at 37°C for 30 days, the dentin discs were dissected in the longitudinal direction of the teeth to examine the treatment surfaces and cutting plane of each disc. The samples were rinsed with water, dehydrated, and sputter-coated with platinum. Subsequently, field-emission scanning electron microscopy (FESEM; SUPRA25; Carl Zeiss, Oberkochen, Germany) assessments were performed to observe changes in the exposed dentinal tubule occlusion after each treatment. The two portion of each dissected disc (number of FESEM image = 10) was observed at magnifications of $\times 2000$, and the occlusion of the dentinal tubules was confirmed by calculating the area ratios of the occluded dentinal tubules (area of occluded tubules/total tubules area) using Image J software (version 1.50; NIH, Bethesda, MD, USA) (<http://imagej.nih.gov/ij/docs/guide/146-29.html>).

In vitro mineralization test

Simulated body fluid (SBF, Biosesang; Seoul, Korea), maintained at a pH of 7.3–7.4, was used to assess in vitro mineralization. First, 100 mg of 368A, 368B, 1840A, and 1840B was added to 15 mL of SBF solution and soaked at 37°C for 1, 10, and 30 days. After soaking, the SBF solution was removed and the samples were washed three times with distilled water for 5 min. After drying the sample at 80°C , the functional groups present were examined by FT-IR measured from 2000 to 600 cm^{-1} at a 4 cm^{-1} resolution.

Statistical analysis

A one-way ANOVA analysis of variance was used to compare FESEM images of dentinal tubule occlusion and acid resistance stability. All statistical analyses were performed using the language R program (R Foundation for Statistical Computing, Vienna, Austria).

Results

Characterization

X-ray diffraction

Figure 1 shows the XRD patterns of the 368A, 368B, 1840A, and 1840B samples. From the small-angle XRD spectra, the 368A and 1840A samples exhibited a single, broad reflection peak, indicating that the samples have a disordered mesostructure. These peaks were not observed in the 368B and 1840B samples, which suggests the formation of a disordered mesostructure due to the coating of BGNs. In the wide-angle XRD, the 368A, 368B, 1840A, and 1840B samples exhibited a non-crystalline structure, suggesting an amorphous state.

Fourier-transform infrared spectroscopy

The chemical compositions of the 368A, 368B, 1840A, and 1840B samples were determined by FT-IR spectroscopy (Fig. 2). In Fig. 2a, silicate adsorption bands at approximately 1060 and 800 cm^{-1} were observed for all samples, representing the symmetric stretching mode and asymmetric stretching vibration of Si–O–Si, respectively. However, in the FT-IR spectra of 368B and 1840B, the Si–O–Si peaks are reduced, which is related to the bioactive glass covering the silica surface. The peak at 1635 cm^{-1} in the 368A spectrum (Fig. 2b) is associated with the Si–O–H vibration (silanol

groups linked to H_2O molecules). Bands at 1223 and 803 cm^{-1} arise from Si–O–Si vibration, and the band at 973 cm^{-1} , from the Si–OH bending deformation. The FT-IR spectrum of 368B is shown in Fig. 2c and is similar to that of 368A. Peaks in the vicinity of 798 cm^{-1} likely arise from the P–O bending of the PO_4^{3-} groups. The weak bands observed at approximately 1489 and 1428 cm^{-1} are related to the residual carbonate groups in the precursor. In Fig. 2d, the FT-IR spectrum for 1840A is very similar to that of 368A, and the FT-IR spectrum for 1840B (Fig. 2e) is very similar to that of 368B.

N_2 adsorption

The porosity of the 368A, 368B, 1840A, and 1840B samples was evaluated using N_2 adsorption-desorption isotherms (Fig. 3). The 368A, 368B, 1840A, and 1840B samples exhibited a type IV isotherm when capillary condensation occurred due to the pore structure. All samples showed a type H4 hysteresis loop, typically seen in a composite of micropores and mesopores. Table 2 shows the results of specific surface area (S_{BET}), pore volume (V_{p}), and pore diameter (D_{p}) determined by the BET and BJH methods. The pore size increased from 1.15 (368A) to 2.51 nm (368B) and 2.30 (1840A) to 3.07 nm (1840B). The specific surface area decreased rapidly from 849.35 (368A) to 266.77 m^2/g (368B) and 634.34 (1840A) to 263.19 m^2/g (1840B). These results show that the pores of 368A and 1840A were filled with BGNs. In addition, the total pore volume decreased from 0.49 (368A) to 0.31 cm^3/g (368B) and 0.73 (1840A) to 0.40 cm^3/g (1840B).

Field-emission transmission electron microscopy

The shapes of the prepared samples were studied using 200 kV FETEM. In the FETEM images (Fig. 4a, c), 368A showed a diameter of 300–400 nm and 1840A a diameter of 150–250 nm. The coated BGN crystals observed in the 368B and 1840B samples exhibited a size of 30–50 nm (Fig. 4b, d).

Fig. 1 a Small-angle XRD patterns of the 368A, 368B, 1840A, and 1840B samples. b Wide-angle XRD pattern of the 368A, 368B, 1840A, and 1840B samples

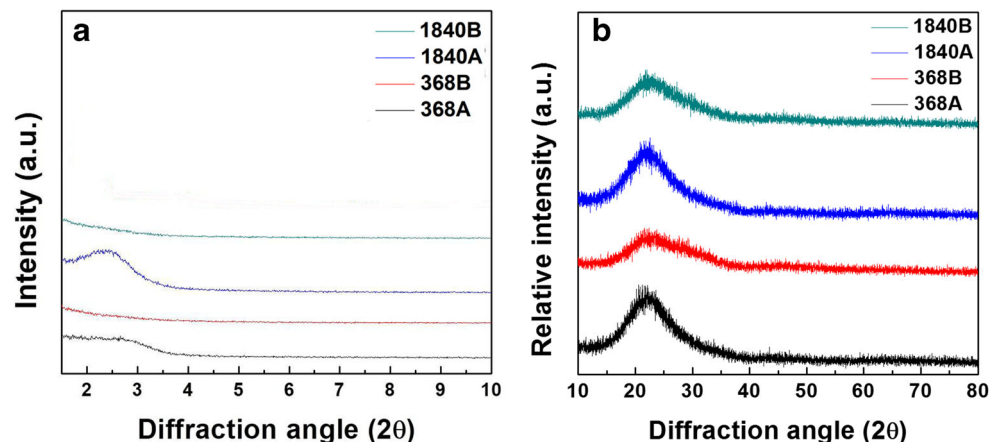
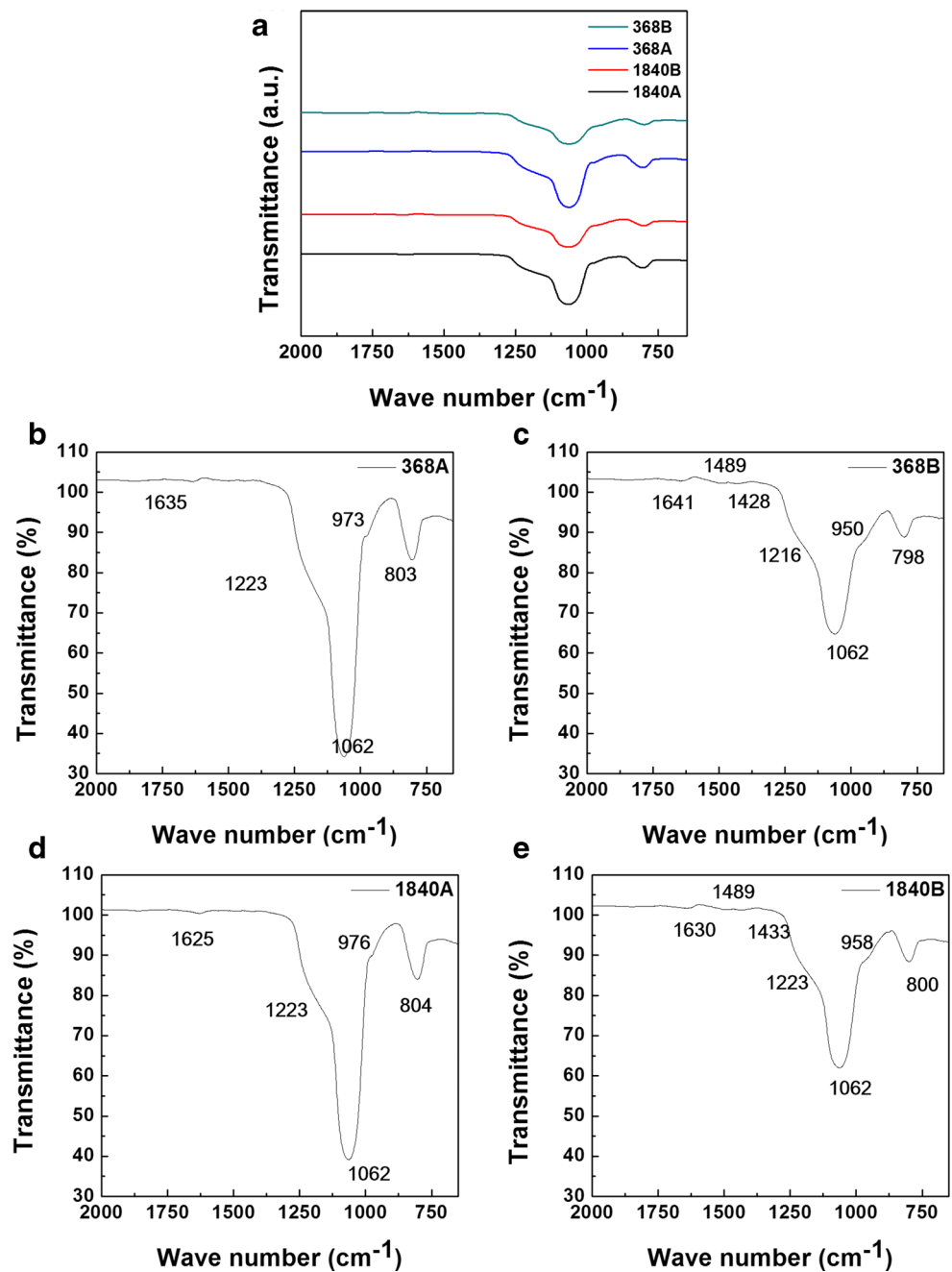


Fig. 2 **a** FT-IR spectra of the 368A, 368B, 1840A, and 1840B samples. **b** The bands of 368A at 1223 and 803 cm^{-1} are from Si–O–Si vibrations and 973 cm^{-1} arises from Si–OH bending deformation. **c** The spectrum of 368B, which is very similar to that of 368A. Peaks in the vicinity of 798 cm^{-1} arise from the P–O bending of the PO_4^{3-} groups. The weak bands observed at approximately 1489 and 1428 cm^{-1} arise from the residual carbonate groups of the precursor. **d** The 1840A spectrum, which is very similar to that of 368A. **e** The spectrum of 1840B, which is very similar to that of 368B



Inspection of the FETEM images reveals that an ordered mesoporous structure was adopted and BGNs were coated in the composite.

FESEM observation of dentinal tubule occlusion and acid resistance stability

Figure 5 shows the effect of dentinal tubule occlusion observed on the top surfaces of groups 1–6 before (A) and 30 days after (B) exposure to 6 wt% citric acid solution for 1 min. The images of group 1 (Fig. 5(A1)) show dentin surface with no smear layer and open dentinal

tubules after immersion in 1 wt% citric acid solution for 20 s and 30 days after exposure to 6 wt% citric acid solution for 1 min (Fig. 5(B1)), the diameters of the dentinal tubules increased. Groups 2 (Fig. 5(A2)), 3 (Fig. 5(A3)), 4 (Fig. 5(A4)), 5 (Fig. 5(A5)), and 6 (Fig. 5(A6)) show each 368A, 368B, 1840A, and 1840B particle, respectively, penetrated and partially occluded the tubules. Thirty days after exposure to 6 wt% citric acid solution for 1 min, groups 2 (Fig. 5(B2)), 3 (Fig. 5(B3)), 4 (Fig. 5(B4)), 5 (Fig. 5(B5)), and 6 (Fig. 5(B6)) show decreased number of particles covering the tubule surfaces.

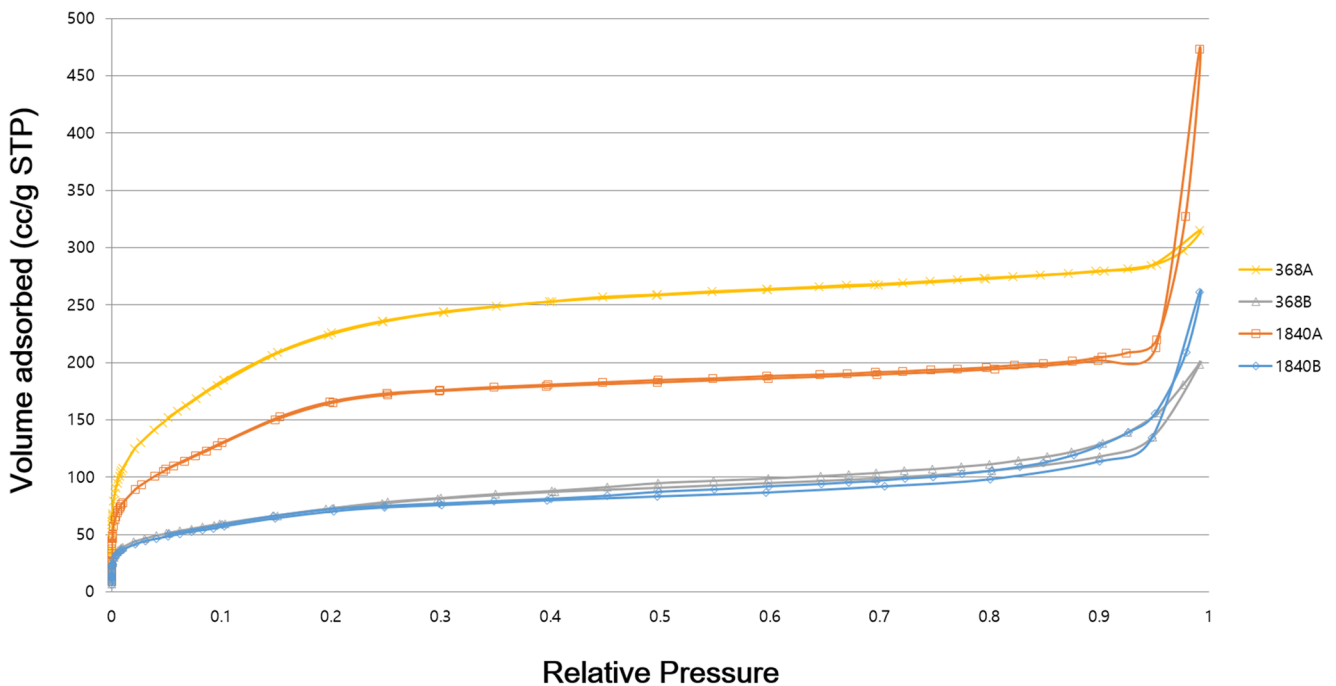


Fig. 3 Nitrogen adsorption-desorption isotherms of the 368A, 368B, 1840A, and 1840B samples

Figure 6 shows the effect of dentinal tubule occlusion observed on the longitudinal surfaces of groups 1–6 before (A) and 30 days after (B) exposure to 6 wt% citric acid solution for 1 min. In group 1, Fig. 6(B1) shows a larger diameter of the dentinal tubule (star) than Fig. 6(A1). Groups 2 (Fig. 6(A2)), 3 (Fig. 6(A3)), and 5 (Fig. 6(A5)) partially filled the dentinal tubules with their particles, respectively. Groups 4 (Fig. 6(A4)) and 6 (Fig. 6(A6)) filled the dentinal tubule walls more densely with particles and occluded the dentinal tubules. After 30 days of exposure to 6 wt% citric acid solution, in groups 2 (Fig. 6(B2)), 3 (Fig. 6(B3)), and 5 (Fig. 6(B5)), the particles disappear which occluded the dentinal tubule orifice. In addition, the depth of MSN particles in the remaining tubules in groups 3 (Fig. 6(B3)) and 5 (Fig. 6(B5)) decreased. In groups 4 and 6, more tubules were occluded than in the other groups and a membrane-like layer completely covering the dentin surface was formed (Fig. 6(B4, B6)).

Table 2 N₂ adsorption results

Samples	S_{BET} (m ² /g)	V_p (cm ³ /g)	D_p (nm)
368A	849.35	0.49	1.15
368B	266.77	0.31	2.30
1840A	634.34	0.73	2.30
1840B	263.19	0.40	3.07

S_{BET} (m²/g) the surface area, V_p (cm³/g) the total pore volume for pores with radii, D_p (nm) average pore radius

Occluded area ratio analysis

Table 3 shows the area ratio of the occluded dentinal tubules before applying the 6 wt% citric acid solution for 1 min in each group. After applying 6 wt% citric acid, the area of occlusion of the dentinal tubules decreased in all groups. No statistically significant difference in the area ratio before the application of 6 wt% citric acid was observed between groups, except for that of the BG group. After the application of 6 wt% citric acid, the area of occlusion decreased for each group. The BG group showed the biggest decrease (20%) in terms of the occlusion area, and occlusion areas in the 368A and 1840A groups were reduced by approximately 17%. The BGN-coated 368B and 1840B groups showed the smallest decrease. Of the five groups, the 1840B group had the least amount of area reduction (7%), and the area of occlusion remaining in the dentinal tubule after acid application was not significantly different from that of the 368B group, though its area was the largest, suggesting high acid resistance stability.

In vitro bioactivity assay

Figure 7 shows the FT-IR spectra, indicating the changes in the composition after exposure of samples to SBF solution for 1, 10, and 30 days. The silicate adsorption bands near 1060 and 800 cm⁻¹ were observed most strongly and silicate-related peaks near 1635, 1223, 973, and 803 cm⁻¹ were observed before treatment with SBF solution, as shown in Fig. 2. In addition to silicate, weak bands at approximately 1489 and 1428 cm⁻¹ were also observed, which are related to the peak

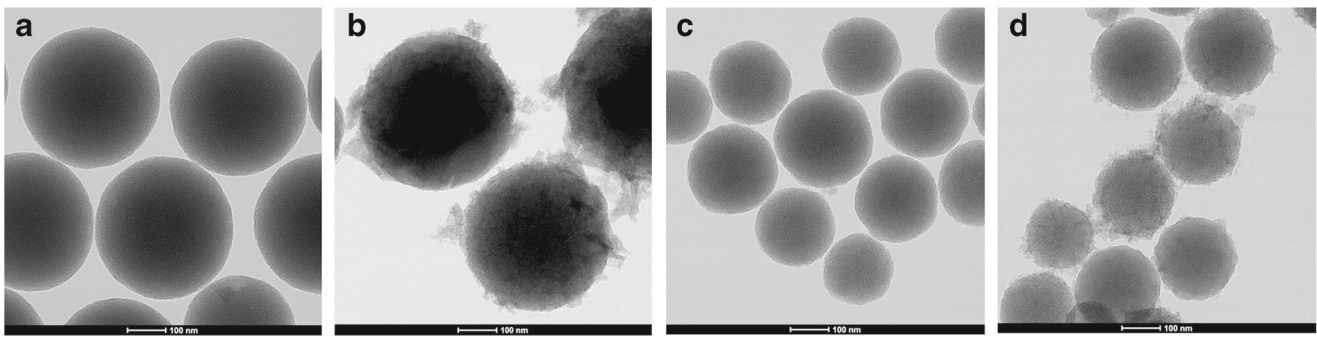


Fig. 4 The 200-kV FETEM images of the **a** 368A, **b** 368B, **c** 1840A, and **d** 1840B samples

of the carbonate groups, and another at approximately 798 cm^{-1} from the PO_4^{3-} groups.

The compositional change of samples after exposure to SBF solution can be seen through a newly formed peak. The 875 (very weak peak), 1350 , and 1738 cm^{-1} peaks are related to the carbonate band and were observed in the 368A/B groups at day 30 and 1840A/B at day 1. The 955 cm^{-1} peak arising from the phosphate group was observed in the 368B group at day 10 and in 1840B at day 1 (the 966 cm^{-1} peak of the SiOH group was observed in groups 368A and 1840A). These FT-IR spectra are similar to the spectra observed for hydroxyapatite [18].

Discussion

Dentin hypersensitivity (DH) is characterized by instantaneous, sharp pain usually caused by heat, vapor, contact, osmotic pressure, or chemical stimulation at the exposed dentin site caused by enamel loss or gingival recession. Among the various DH treatments available that are based on the hydrodynamic mechanism, the method that blocks fluid flow by effectively occluding exposed dentinal tubules has been introduced as an effective treatment strategy for DH [19, 20].

The aim of this study was to investigate the effect of occlusion and remineralization of dentinal tubules by controlling the MSN particle size of the BGN@MSN biocomposite material, which is known to be effective in the dentinal tubule sealing [12]. According to the results of this study, the null hypothesis was rejected. XRD, FT-IR, N_2 adsorption-desorption isotherms, and FETEM were used to determine the sizes of the prepared MSN particles (368A, 1840A) which were synthesized according to the concentration difference of TEOS and whether BGN was well-coated on the MSNs (368A, 1840B). The particle sizes of 368A and 1840A determined through FESEM observation and N_2 adsorption were different (Fig. 4a, c), which indicated that the surface area also differed (Table 1). This is consistent with a previous study conducted by Kambara et al. [15]. For the 368B and 1840B samples, BGN surrounded the structure of the 368A and 1840A MSNs without infringement (Fig. 4b, d). This is

because MSNs have a large surface area and pore volume with excellent surface properties, and their high surface porosity provides nucleation sites during the synthesis process, creating a unique structure where BGN surrounds the MSN surface [21].

From the N_2 adsorption-desorption isotherms, the surface area before BGN coating was larger for 368A than 1840A, but 1840A was larger than 368A in terms of total pore volume and average pore radius. After BGN coating, both surface areas decreased by more than half and the total pore volume decreased because the mesoporous entrances were blocked by BGN covering the MSN surface [21].

To determine the effect of the different sizes of BGN@MSN particles on the occlusion of dentinal tubules, we applied BG, the most commonly used treatment for DH, and synthesized the 368A, 386B, 1840A, and 1840B samples on prepared dentin discs and evaluated the morphological changes of dentinal tubules by FESEM. BG, as a control material, induces incremental changes in remineralization and osteoconductivity through ion release [11], and the resulting hydroxycarbonate apatite precipitate mechanically occludes the dentinal tubules [22]. However, in the BG control group, the decomposition of Ca^{2+} and PO_4^{3-} is partially blocked by the glass particles and the action of the bioactive glass is delayed, resulting in partially incomplete occlusion of dentinal tubules (Fig. 6(A2)). The 368A and 1840A samples are MSNs that penetrate deeper into the dentinal tubules than the BG group. Both 1840A and 368A could not closely occlude the dentinal tubules, as both penetrated the target, and 1840A with a smaller size penetrated deeper than the 368A particles (Fig. 6(A3, A5)). The 368B and 1840B samples coated with BGN formed clumps in the dentinal tubules and more closely occluded the dentinal tubule wall (Fig. 6(A4, A6)). Thus, BGN fills the spaces generated between the MSN particles.

In DH treatment, resistance to dietary acid is important for maintaining long-term therapeutic effects. Therefore, acid resistance is an important criterion for the occlusion effect of dentinal tubules [23]. Citric acid, which is capable of dissolving calcium phosphate [24], is a common ingredient in many foodstuffs, and 6 wt% citric acid solution (pH 1.5) was used in the study [25]. The morphological changes of the dentinal

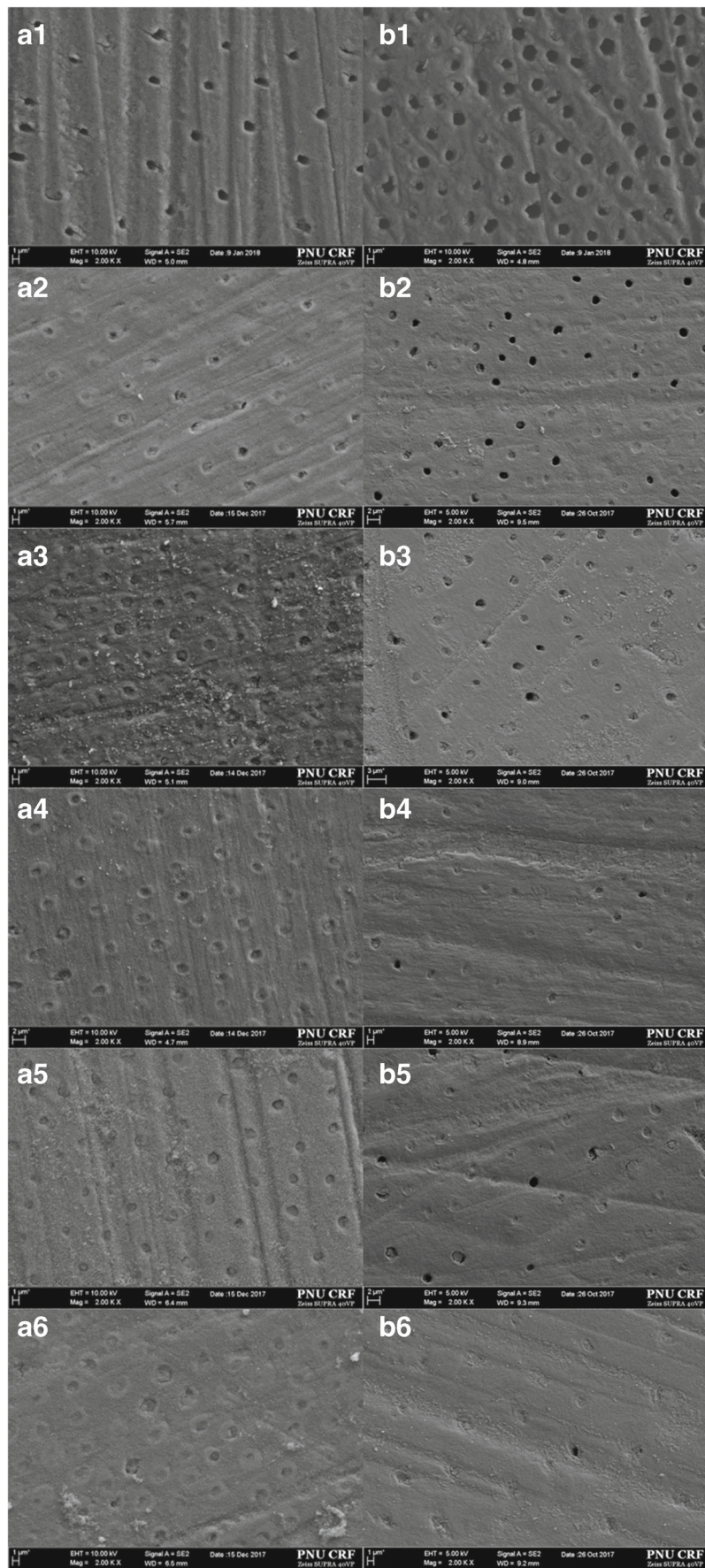


Fig. 5 FESEM images ($\times 2000$) of the top sides of the samples which were used to determine the tubule-occluding effect in each group. A1–A6 are images before exposure to 6 wt% citric acid solution and B1–B6 are images 30 days after exposure to 6 wt% citric acid solution for 1 min. In group 1 (control), B1 shows larger diameter of the dentinal tubule than A1. In group 2 (BG), 3 (368A), 4 (368B), 5 (1840A), and 6 (1840B), B2–B6 show a decreased number of particles occluding the dentinal tubule than A2–A6

tubules observed via FESEM imaging before and after exposure to 6 wt% citric acid solution were evaluated. Dentin discs without treatment increased the size of the dentinal tubules after exposure to 6 wt% citric acid solution (Figs. 5 and 6(B1)). This is because of the removal of smear layer and erosion of peritubular dentin in an acidic environment [25]. For the BG-applied dentin disc, a significant number of BGs blocking the dentinal tubules were removed, especially the ones around the tubule orifice, showing reduced depth of occlusion (Fig. 6(B2)).

The area ratio of the occluded dentinal tubules was also reduced by approximately 20% (Table 3). It is well known that when BG is exposed to an acidic environment, the calcium phosphate deposited in the dentinal tubules is eluted, and the tubules are reopened.

The ratios of dentinal tubule occlusion were similar in the other groups, except for BG, but the acid resistance stability differed depending on BGN coating after exposure to the 6 wt% citric acid solution. For the 368A and 1840A samples, the occlusion areas of dentinal tubules were reduced by approximately 17% ($P < 0.05$, Table 3), presumably because of the acid resistance of mesoporous silica. This stability can be explained by the adherence and closure of the dental tubule by the hydroxyl group that binds silica to the calcium receptors of the dentin surface [26]. However, the 368B sample showed a reduction of approximately 10% and 1840B, approximately 7% ($P < 0.05$, Table 3), after BGN coating. It is presumed that this increased acid resistance stability is due to the coating of BGN which filled the spaces between MSN particles in the 368B and 1840B samples, although considerable spaces remained between the 368A and 1840A particles. In 368A and 1840A, the particles in the tubule orifice disappeared and the depth of occlusion decreased. On the other hand, in 368B and 1840B, most of the remaining dentinal tubules occluded, and the shapes of the particles changed, forming a membrane-like layer (box) completely covering the dentin surface (Fig. 6(B3–B6)). This apatite-like layer is thought to be responsible for the increased acid resistance stability.

While there was no statistical difference from that of 368B, the dentinal tubule occlusion ratio of 1840B was the highest after acidic challenge, and in vitro bioactivity assays were performed to confirm this finding. The 368A, 368B, 1840A, and 1840B samples were soaked in a SBF solution for 1, 10, and 30 days, and the composition of the solution was examined by FT-IR (Fig. 7a–d). The formation of the apatite-like

Fig. 6 FESEM images ($\times 2000$) of the longitudinal sides of the samples which were used to determine the tubule-occluding effect in each group. A1–A6 are images before exposure to 6 wt% citric acid solution and B1–B6 are images 30 days after exposure to 6 wt% citric acid solution for 1 min. In group 1 (control), A1 shows a dentinal tubule with its smear layer removed (star) and B1 shows a large diameter of the dentinal tubule (star). In group 2 (BG), A2 shows partially occluded dentinal tubules with a depth of 1–2 μm (arrows) and B2 shows a decreased number of particles occluding the dentinal tubule. In group 3 (368A), A3 shows dentinal tubules partially occluded at a depth of 2–3 μm (arrows) and the particles in the tubules are scattered. B3 shows reduced particles occluding the dentinal tubules, which disappeared particles in the tubule orifice. Also, the occlusal depth is reduced. In group 4 (368B), A4 shows dentinal tubules were completely occluded by the particles at a depth of 4–5 μm (arrows). B4 shows most dentinal tubules were occluded, and the shape of the particles changed to form a membrane-like layer (box) completely covering the dentin surface. In group 5 (1840A), A5 is partially occluded with particles with dentinal tubules scattered at a depth of 2–5 μm (arrows) and B5 shows reduced particles occluding the dentinal tubule with disappeared particles in the orifice of the dentinal tubule, and decreased occlusion depth. In group 6 (1840B), A6 shows dentinal tubules were 4–5 μm deep (arrows) and the particles were clustered together and occluded the dentinal tubules. B6 shows most of the dentinal tubules were closed, and the shape of the particles changed to form a membrane-like layer (box) completely covering the dentin surface

layer can be inferred through the carbonate and phosphate bands. Carbonate bands (875, 1350, and 1738 cm^{-1} peaks) were produced in all groups, but in 1840A and 1840B, the band was observed at day 1, whereas for 368A and 368B, the band was observed at day 30. Thus, it can be deduced that the particle size influenced the time required for formation of the carbonate band. This is similar to a previous study in which nanometer-sized bioactive glass (20–50 nm) led to increased dentin remineralization compared to micrometer-sized bioactive glass [27]. This is thought to be related to the increased mechanical maintenance due to tight attachment [28]. On the other hand, phosphate bands (955 cm^{-1} peak) were not observed in 368A or 1840A but were observed in 368B at day 10 and in 1840B at day 30. It is conceivable that the composition of the particles affects the formation of phosphate bands. The presence of BGN also affects the formation of phosphate and even more so in the case of 1840B whose particles are smaller. This indicates that an apatite-like layer was formed in the 368B and 1840B samples, which is more effective in 1840B whose particles are smaller. This is consistent with recent findings that pure mesoporous silica materials (such as MCM-41) do not exhibit bioactive behavior [29], but phosphorous- or bioactive glass-doped mesoporous silica materials induce the formation of apatite layers [30, 31].

In summary, two sizes of BGN@MSN biocomposites were successfully synthesized, which exhibited acid resistance stability and remineralization capability with successful occlusion of exposed dentin tubules. Comparing the different-sized particles of 368B and 1840B, 1840B, having smaller particle size and larger surface area and pore volume, may be more effective in treating DH in clinical applications.

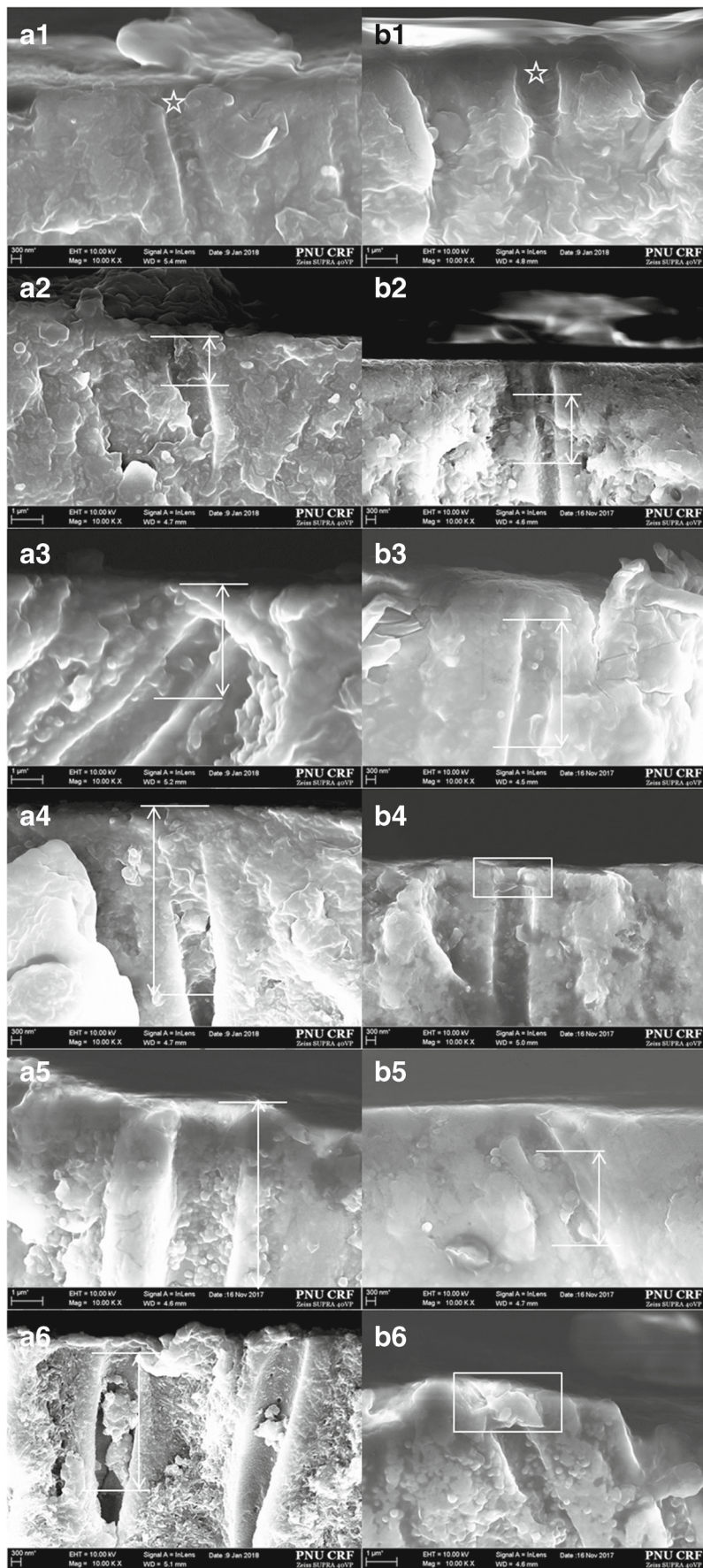


Table 3 Area ratio of the occluded dentinal tubule

Groups	Occluded area (%)	
	Before acid challenge	After acid challenge
Control	–	–
BG	78.30 ± 7.68 ^d	58.47 ± 2.98 ^f
368A	86.68 ± 10.45 ^{abc}	69.70 ± 5.23 ^e
368B	89.08 ± 6.28 ^{ab}	79.56 ± 8.71 ^{cd}
1840A	87.70 ± 8.55 ^{ab}	70.05 ± 7.28 ^e
1840B	89.87 ± 2.21 ^a	82.60 ± 3.28 ^{bcd}

*One-way ANOVA was performed. The same superscript indicates that the differences between values are not significant; *P* < 0.05

However, further in vivo studies should be performed to confirm these results. Since this was only in vitro study, there were limitations to simulate the intraoral environment. From the in vivo study, other factors including intraoral temperature,

dental biofilm, salivary proteins, food debris, and bacterial products should be considered. This would increase the possibility of developing long-term and more effective DH treatment methods.

Conclusion

Long-term stability to acid challenge after dentinal tubule occlusion is an important factor in the treatment of DH. Particle size and surface area are thought to significantly affect this process. Therefore, in this study, we synthesized two different sizes of MSN particles coated with BGN to study the long-term stability to acid challenge after the occlusion and remineralization of dentinal tubules. The different-sized 368A and 1840A MSNs and 368B and 1840B MSN coated with BGN were successfully synthesized by the Stöber and sol-gel methods, respectively, and characterized by XRD, FT-

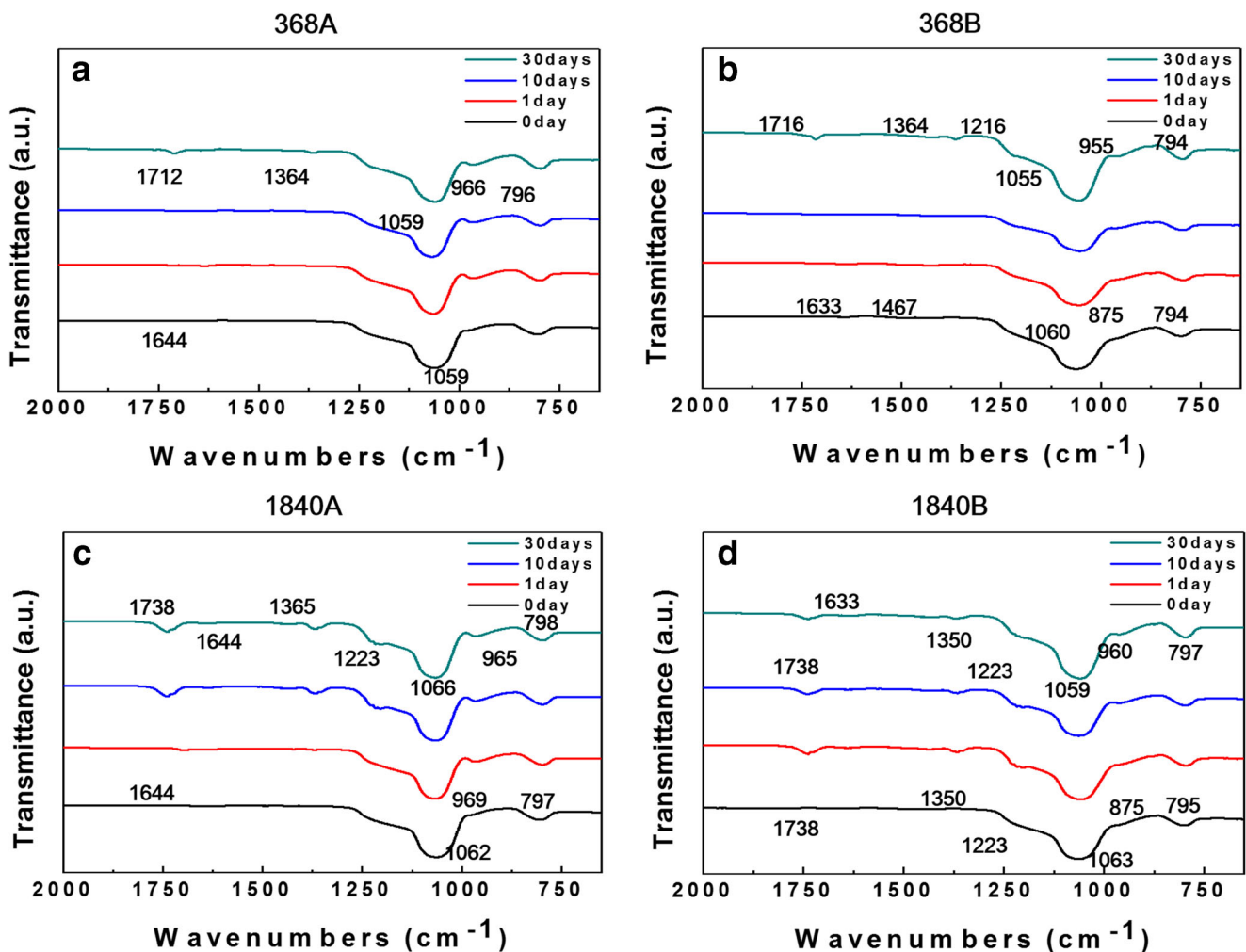


Fig. 7 FT-IR spectra of the compositional changes upon exposure to SBF solution of groups 368A (a), 368B (b), 1840A (c), and 1840B (d) for 1, 10, and 30 days. **a** 368A: 875, 1350, and 1738 cm⁻¹ peaks on day 30. **b** 368B: 955 cm⁻¹ peak appears at day 10 and 875, 1350, 1738 cm⁻¹ peaks

appear at day 30. **c** 1840A: 875, 1350, 1738 cm⁻¹ peaks appear at day 1. **d** 1840B: 875, 1350, 1738 cm⁻¹ peaks as well as the 955 cm⁻¹ peak appear at day 1

IR, FETEM, and BET. Both 368B and 1840B samples successfully occluded dentinal tubules and were acid-resistant, retaining their remineralization capability. During the in vitro bioactivity assay and dentinal tubule occlusion experiments, 1840B, with its small particle size and large surface area and pore volume, may be more effective in treating DH in clinical applications.

Funding This work supported by the National Research Foundation of Korea (NRF) grant funded by the Korea government (2018R1D1A1B07042098).

Compliance with ethical standards

Conflict of interest YI Kim has received research grants from the National Research Foundation of Korea (NRF) for this study. All authors declare that they have no competing interest.

Ethical approval The study was reviewed and approved by the Institutional Review Board of Pusan National University Dental Hospital (PNUDH-2016-033).

Informed consent Informed consent was obtained from all individual participants included in the study.

References

- Rees JS, Addy M (2004) A cross-sectional study of buccal cervical sensitivity in UK general dental practice and a summary review of prevalence studies. *Int J Dent Hyg* 2(2):64–69. <https://doi.org/10.1111/j.1601-5029.2004.00068.x>
- Brännstrom M, Astrom A (1964) A study on the mechanism of pain elicited from the dentin. *J Dent Res* 43(2):619–625. <https://doi.org/10.1177/00220345640430041601>
- Orchardson R, Gilliam D (2006) Managing dentin hypersensitivity. *J Am Dent Assoc* 137(7):990–998. <https://doi.org/10.14219/jada.archive.2006.0321>
- Krahwinkel T, Theiss P, Willershausen B (2001) Clinical effectiveness of a potassium chloride containing chewing gum in the treatment of hypersensitive teeth. *Eur J Med Res* 6(11):483–487
- Morris MF, Davis RD, Richardson BW (1999) Clinical efficacy of two dentin desensitizing agents. *Am J Dent* 12(2):72–76
- Pillon FL, Romani IG, Schmidt ER (2004) Effect of a 3% potassium oxalate topical application on dentinal hypersensitivity after subgingival scaling and root planing. *J Periodontol* 75(11):1461–1464. <https://doi.org/10.1902/jop.2004.75.11.1461>
- Ananthakrishna S, Raghu TN, Koshy S, Kumar N (2012) Clinical evaluation of the efficacy of bioactive glass and strontium chloride for treatment of dentinal hypersensitivity. *J Interdiscipl Dent* 22(2):92–97. <https://doi.org/10.4103/2229-5194.100600>
- Mitchell JC, Musanje L, Ferracane JL (2011) Biomimetic dentin desensitizer based on nano-structured bioactive glass. *Dent Mater* 27(4):386–393. <https://doi.org/10.1016/j.dental.2010.11.019>
- Tang F, Li L, Chen D (2012) Mesoporous silica nanoparticles: synthesis, biocompatibility and drug delivery. *Adv Mater* 24(12):1504–1534. <https://doi.org/10.1002/adma.201104763>
- Huang X, Young NP, Townley HE (2014) Characterisation and comparison of mesoporous silica particles for optimised drug delivery. *Nanomater Nanotechnol* 4(4):21–36. <https://doi.org/10.5772/58290>
- Tian L, Peng C, Shi Y, Guo X, Zhong B, Qi J et al (2014) Effect of mesoporous silica nanoparticles on dentinal tubule occlusion: an in vitro study using SEM and image analysis. *Dent Mater J* 33(1):125–132. <https://doi.org/10.4012/dmj.2013-215>
- Jung JH, Kim DH, Yoo KH, Yoon SY, Kim Y, Bae MK, Chung J, Ko CC, Kwon YH, Kim YI (2018) Dentin sealing and antibacterial effects of silver-doped bioactive glass/mesoporous silica nanocomposite: an in vitro study. *Clin Oral Invest*. <https://doi.org/10.1007/s00784-018-2432-z>
- Erol-Taygun M, Zheng K, Boccaccini AR (2013) Nanoscale bioactive glasses in medical applications. *Int J Appl Glas Sci* 4:136–148. <https://doi.org/10.1111/ijag.12029>
- Webster TJ, Ergun C, Doremus RH, Siegel RW, Bizios R (2000) Enhanced functions of osteoblasts on nanophase ceramics. *Biomaterials* 21:1803–1810. [https://doi.org/10.1016/S0142-9612\(00\)00075-2](https://doi.org/10.1016/S0142-9612(00)00075-2)
- Stöber W, Fink A, Bohn E (1968) Controlled growth of monodisperse silica spheres in the micron size range. *J Colloid Interface Sci* 26:62–69. [https://doi.org/10.1016/0021-9797\(68\)90272-5](https://doi.org/10.1016/0021-9797(68)90272-5)
- Xia W, Chang J (2007) Preparation and characterization of nano-bioactive-glasses (NBG) by a quick alkali-mediated sol–gel method. *Mater Lett* 61(14–15):3251–3253. <https://doi.org/10.1016/j.matlet.2006.11.048>
- Pei D, Liu S, Huang C, du X, Yang H, Wang Y, Deng D (2013) Effect of pretreatment with calcium-containing desensitizer on the dentine bonding of mild self-etch adhesives. *Eur J Oral Sci* 121(3pt1):204–210. <https://doi.org/10.1111/eos.12047>
- Liga BC, Natalija B (2012) Infrared spectroscopy - materials science, engineering and technology. Prof. Theophanides Theophile, editors. *Research of Calcium Phosphates Using Fourier Transform Infrared Spectroscopy*. InTech. 123–148. <https://doi.org/10.5772/36942>
- Schmidlin PR, Sahrman P (2013) Current management of dentin hypersensitivity. *Clin Oral Investig* 17(Suppl 1):S55–S59. <https://doi.org/10.1007/s00784-012-0912-0>
- Pashley DH (1994) Dentin permeability and its role in the pathobiology of dentin sensitivity. *Arch Oral Biol* 39(Supplement):S73–S80. [https://doi.org/10.1016/0003-9969\(94\)90191-0](https://doi.org/10.1016/0003-9969(94)90191-0)
- Wang Y, Zhao Q, Han N, Bai L, Li J, Liu J, Che E, Hu L, Zhang Q, Jiang T, Wang S (2015) Mesoporous silica nanoparticles in drug delivery and biomedical applications. *Nanomedicine* 11(2):313–327. <https://doi.org/10.1016/j.nano.2014.09.014>
- Chiang YC, Chen HJ, Liu HC, Kang SH, Lee BS, Lin FH, Lin HP, Lin CP (2010) A novel mesoporous biomaterial for treating dentin hypersensitivity. *J Dent Res* 89(3):236–240. <https://doi.org/10.1177/0022034509357148>
- Wang Z, Sa Y, Sauro S, Chen H, Xing W, Ma X, Jiang T, Wang Y (2010) Effect of desensitising toothpastes on dentinal tubule occlusion: a dentine permeability measurement and SEM in vitro study. *J Dent* 38(5):400–410. <https://doi.org/10.1016/j.jdent.2010.01.007>
- Xu Z, Neoh KG, Kishen A (2008) Monitoring acid-demineralization of human dentine by electrochemical impedance spectroscopy (EIS). *J Dent* 36(12):1005–1012. <https://doi.org/10.1016/j.jdent.2008.08.007>
- Reis C, De-Deus G, Leal F, Azevedo E, Coutinho-Filho T, Paciomiak S (2008) Strong effect on dentin after the use of high concentrations of citric acid: an assessment with co-site optical microscopy and ESEM. *Dent Mater* 24(12):1608–1815. <https://doi.org/10.1016/j.dental.2008.03.027>
- West NX, Hughes JA, Addy M (2002) Dentine hypersensitivity: the effects of brushing toothpaste on etched and unetched dentine in vitro. *J Oral Rehabil* 29(2):167–174. <https://doi.org/10.1046/j.1365-2842.2002.00851.x>

27. Vollenweider M, Brunner TJ, Knecht S, Grass RN, Zehnder M, Imfeld T, Stark WJ (2007) Remineralization of human dentin using ultrafine bioactive glass particles. *Acta Biomater* 3(6):936–943. <https://doi.org/10.1016/j.actbio.2007.04.003>
28. Curtis AR, West NX, Su B (2010) Synthesis of nanobioglass and formation of apatite rods to occlude exposed dentine tubules and eliminate hypersensitivity. *Acta Biomater* 6(9):3740–3746. <https://doi.org/10.1016/j.actbio.2010.02.045>
29. Izquierdo-Barba I, Ruiz-González L, Doadrio JC, González-Calbet JM, Vallet-Regí M (2005) Tissue regeneration: a new property of mesoporous materials. *Solid State Sci* 7(8):983–989. <https://doi.org/10.1016/j.solidstatesciences.2005.04.003>
30. Horcajada P, Rámila A, Boulahya K, González-Calbet J, Vallet-Regí M (2006) Bioactivity in ordered mesoporous materials. *Solid State Sci* 6(11):1295–1300. <https://doi.org/10.1016/j.solidstatesciences.2004.07.026>
31. Vallet-Regí M, Izquierdo-Barba I, Rámila A, Pérez-Pariente J, Babonneau F, González-Calbet JM (2005) Phosphorous-doped MCM-41 as bioactive material. *Solid State Sci* 7(2):233–237. <https://doi.org/10.1016/j.solidstatesciences.2004.10.038>